

## FEDSM-ICNMM2010-31063

### 2D MEASUREMENT AND SIMULATION OF MICROPARTICLE CROSS-SECTIONAL DISTRIBUTION BY MICRO PROCESS TOMOGRAPHY

Je-Eun Choi<sup>\*1</sup>, Tong Zhao<sup>2</sup>, Masahiro Takei<sup>2</sup>

<sup>1</sup>Department of Mechanical Engineering, Graduate School of Science and  
Technology, Nihon University  
email: cje\_0205@hotmail.com, 1-8-14, Kanda, Surugadai, Tokyo, 101-8380 JAPAN  
<sup>2</sup>Department of Mechanical Engineering, Nihon University, Tokyo, JAPAN

#### ABSTRACT

The application of micro process tomography to microchannels is considered in this paper. Using the micro process tomography system in microchannel, a particle distribution image can be obtained in a two phase flow. Based on the reconstructed image, it is easy to estimate the particle movement in a fluid flow. A novel microchannel system is designed for electrical process tomography that includes 60 electrodes distributed cross-sectional at five positions. The particle and water were injected into the microchannel, and then the capacitance of the fluid flow was measured at cross-section of microchannel. The result showed the 2D image of particle distribution of cross-section in the microchannel. Also, cross-sectional images of the particle distribution of a two phase flow are simulated.

#### 1. INTRODUCTION

Multiphase flow in a microchannel has attracted attention as a result of its wide range of applications, which include medical and biomedical applications, as well as chemical separations ([1], [2]). The emergence of micro-electro-mechanical-systems (MEMS) technology [3] has generated tremendous interest in micro-scale two phase flow dynamics[4]. In order to fabricate the microchannel and to enhance the industrial efficiency, the particle concentration distribution inside the microchannel must be known. A number of studies have investigated measurement of the particle concentration distribution inside the microchannel using micro particle image velocimetry (micro-PIV) and micro laser induced fluorescence (micro-LIF) [5]. Micro-PIV is used in order to quantify the particle liquid two phase flow patterns for the measurement of particle concentration distribution in a horizontal cross-section of a microchannel [6]. Micro-LIF is commonly used in direct microfluid visualization in a horizontal cross-section [7]. These methods are types of optical visualization; however, the optical visualization is not applicable for the measurement of dense

particle concentration distribution within a vertical cross-section because the optical beam is scattered.

An electrical computed tomography has high possibility to visualize the dense particle concentration distribution in the particle liquid two phase flow in the vertical cross-section. The electrical computed tomography is used for visualization of dielectric media in the case of electrical capacitance tomography (ECT) and conducting media in the case of electrical resistance tomography (ERT) in the vertical cross-section of a large channel [8]. ECT is a technique for obtaining information about the particles concentration distribution of two phase flow by measuring the capacitance between electrodes around the channel [9]. In the past, many researches published already the results of particle distributions in a large scale pipe using capacitance tomography to produce a cross-sectional image of pipe ([10], [11]). This study only showed that the tomography process is a typical for industry applications. ERT is used to evaluate the dynamic behavior of the particle concentration distribution of particle liquid two phase flow by measuring the voltages between electrodes around the channel [12].

New applications are beginning to emerge from miniature sensors in the electrical computed tomography. Griffiths et al. reported a circular array of 16 electrodes that was developed for a miniature sensor in the electrical computed tomography [13]. Also, York et al. [14, 15] showed the 16 electrodes of one cross-section in a miniature sensor by silicon etching, and reconstructed the concentration of multiphase flow in the one cross-section by ECT. However, the miniature sensors are available for the only hole type cross-section in multiphase phase flow. Therefore, the miniature sensors need pipe type and several cross-sections to visualize the spatial transition of the particle concentration distribution in the microchannel.

In this research, using the micro process tomography system in microchannel, a particle distribution image can be obtained in a two phase flow. Based on the reconstructed image, it is

easy to estimate the particle movement in a fluid flow. A novel microchannel system is designed for electrical process tomography that includes 60 electrodes distributed cross-sectional at five positions. The particle and water were injected into the microchannel, and then the capacitance of the fluid flow was measured at cross-section of microchannel. The result showed the 2D image of particle distribution of cross-section in the microchannel. Also, cross-sectional images of the particle distribution of a two phase flow are simulated.

## 2. NOVEL MICROCHANNEL

### 2.1 Manufacturing process of microchannel

The following section describes the fabrication processes of the microchannel. The microchannel has five measurement cross-sections and embeds 12 electrodes in each cross-section for the micro process tomography application.

The microchannel material is quartz glass (width: 2cm, thickness: 200 $\mu$ m) whose characteristics are high heat resistance, transparency through a microscope, strong acid resistance and chemical reactive resistance. The electrode material is platinum wire (width: 200 $\mu$ m, thickness: 0.25 $\mu$ m) whose characteristics are high electrical conductivity, high corrosive resistance, strong acid resistance and chemical reactive resistance. Therefore, this microchannel is considered not only for a common multiphase flow but also for heat transfer process and chemical reaction as well.

The microchannel is fabricated by MEMS processes. Figure 1 shows the fabrication processes of the microchannel in the cross-section: the fabrication processes has six steps. First, the master layers are fabricated by deposition of platinum wire on quartz glass using photolithography [see Fig.1 Step (1)] [16]. The second step is a sandwich compression of the master layer and the quartz glass for making a first electrode layer [see Fig.1 Step (2)]. The third step is a sandwich compression of the first electrode layer and another master layer made by Step (1) for making a second electrode layer. The third electrode layer obtained by repeating the same process is thinned to the 100 $\mu$ m thickness by chemical mechanical polishing [see Fig.1 Step (3)]. The fourth step is the micro mechanical processing called a triangle-shape drilling for making the flow groove [see 1 Step (4)]. The processes until the fourth step is the fabrication processes of the upper electrode layer in the microchannel. The lower electrode layer is obtained by repeating the same process from Steps (1) to (4) [see Fig.1 Step (5)]. The last step is a compression between the upper electrode layer and the lower electrode layer for the microchannel [see Fig.1 Step (6)]. Figure 2 shows the 3D view of complete microchannel embedding 60 electrodes. It has five cross-sections with 6 electrode layers. The distance between two cross-sections is 5mm. Figure 3(a) is the assembly of the microchannel with a transparent acrylic cover. The microchannel has three inlets in the left side of the cover for the flow injection, three outlets in the right side of the cover for the flow discharge. Figure 3(b-1) shows three overlapped electrodes with vertical 200 $\mu$ m clearance in the upper electrode layer from the top view of the microchannel. The electrodes face to the wall of diamond shape groove. Figure 3(b-2) shows the tail part of the overlapped electrodes, separating to three horizontal positions for easy measurement handling.

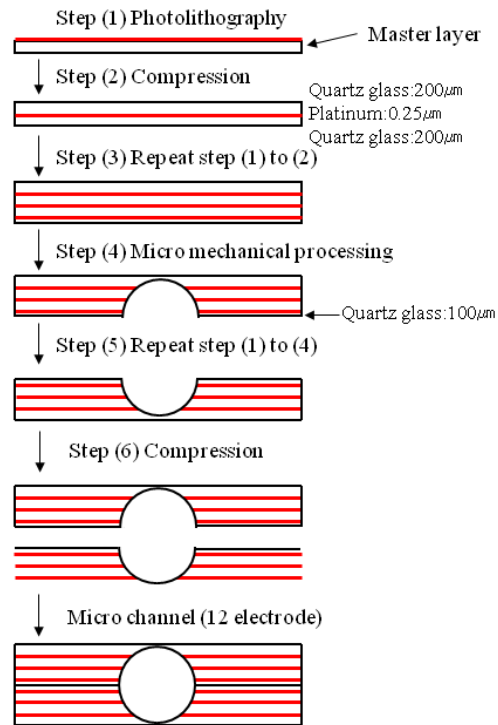


Fig.1 Manufacturing process of microchannel

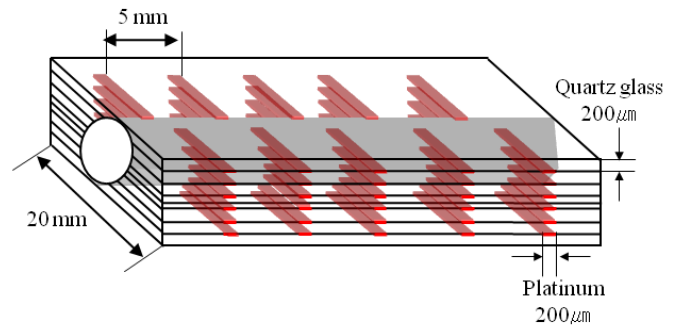


Fig.2 3D view of complete microchannel with embedding 60 electrodes

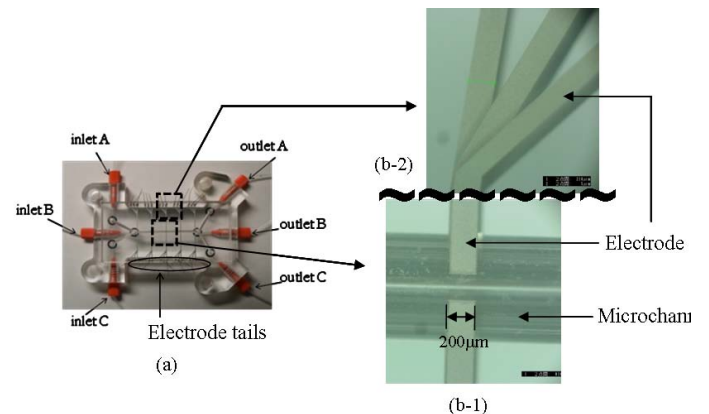


Fig. 3 (a) The assembly of the microchannel with a transparent acrylic cover (b-1) three overlapped electrodes with the microchannel. (b-2) the tail part of the overlapped electrodes

## 2.2 Set up the microchannel connector

Microchannel connector was comprised of two couples patterning board, spring pin, center board and pin connector. Fig.4 shows the picture of microchannel connector with microchannel. The patterning board has 16 pins commercial connector with 15 spring pins. From the patterning board, it can connect to electrode and send a measurement data over the data acquire machine. Spring pins are connected electrodes and patterning board can used commercial connector. The total dimension of this connector system with microchannel is  $140 \times 70 \times 14$  (L×D×H) mm. The patterning board is an application-specific electric circuit for measurement data in our microchannel. It has advantage of stability acquire measurement data, before the system is measured instability data. Because, electrode tails is connected directly to the electric wire by using glue. The electrode tails are easily off to microchannel and if that happens, microchannel cannot measure the data. Therefore, microchannel needs to connect system for a stable measurement. The alternative plan is that the electrode tails part removed then make the small hole in the microchannel. The small holes fill up tartar with lead by mixture. Next step is put a spring pin on a hole of microchannel. In this microchannel connector, it can measured data at the same time. Also, it is very stable method than before system by oneself making.

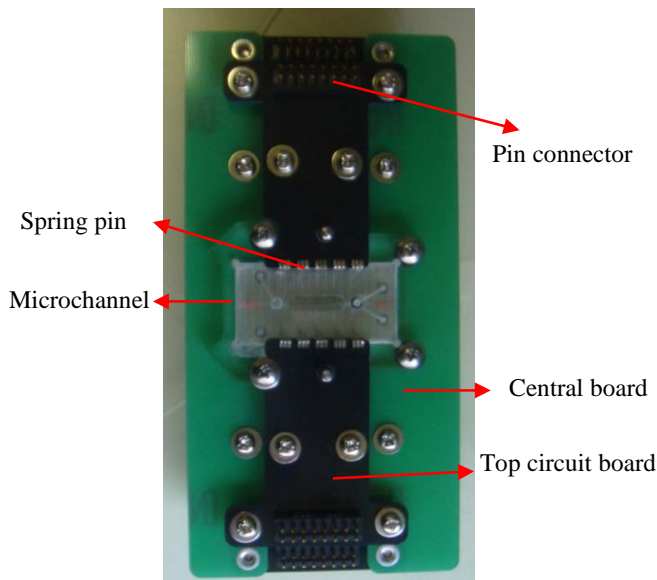


Fig.4 Microchannel system

## 3. EXPERIMENT OF MICROCHANNEL

### 3.1 Experimental setup

The experimental equipment consists of the microchannel system, micro pump, a capacitance measurement system, and a computer as shown in Fig. 5. Figure 6 (a) shows the twelve electrode positions in the cross-section of the microchannel. In the case of 12 electrodes and  $32 \times 32 = 1024$  pixels in the cross-section, as shown in Fig.6 (b). The electrodes are clockwise numbered from the right bottom position #1. The y-axis is the

spanwise direction, the z-axis is the vertical direction. Figure 7 shows the microchannel geometry in the microchannel system. The cross-sectional electrodes are located at the five position of the main flow direction from the cross-sections A to E. The cross-section A is the right edge of the inlets A and C. The distance of the straight part is 20mm from the electrode center of the cross-section A to the electrode center of the cross-section E at each 5mm interval. The x-axis is the main flow direction. The origin point of the coordinate system is the focus point between center of main flow direction and the electrode center of the cross-section A. The two inlets A and C, two outlets A and C are used for the flow injection and the flow discharge respectively. The micro pumps (IC3100 [KDS100], KD Scientific, USA) are an automatic dispenser and control the flow rate to the microchannel inlets. The capacitance measurement system (PTL300, UK) measures the electrical capacitance in the two phase flow in the microchannel system, which sends the electrical capacitance data to the computer.

In the experimental condition, the deionized water ( $2M\Omega$ ) was injected into the inlet A, and the particle flow 3% was injected into the inlet C. The micro particle distribution was measured in the cross-section C. The particle diameter is  $1.3\mu\text{m}$ , and the particle material is spherical polystyrene. The flow rate is 0.001 ml/s, it is corresponded to Poiseuille flow region at low Reynolds number ( $Re=150$ ). The sampling time of each measurement data is 10 seconds: the sampling number is two hundred times per one second.

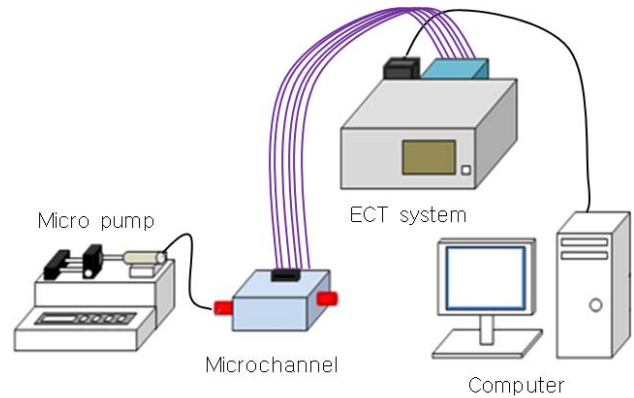


Fig.5 Experiment setup

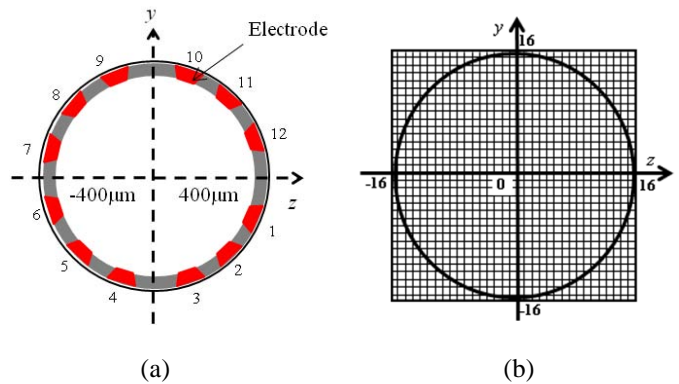


Fig.6 (a) Electrode position in the cross-section (b)  $32 \times 32$  space resolution in the cross-section

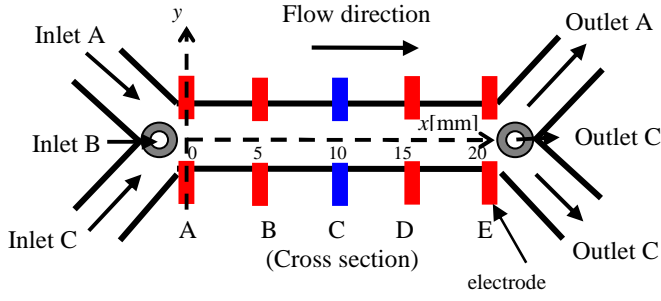


Fig.7 Geometry of the microchannel

#### 4. SIMULATION OF MICROPARTICLE DISTRIBUTION

##### 4.1 Microparticle phase

In this mathematical model, the microparticle phase is treated as a discrete phase that is described by a conventional discrete element method (DEM). Movement of individual microparticle is evaluated by Newton's equation of motion, which includes the effects of gravitational force, contact force, and fluid force. The translational and rotational motions of a particle at any time,  $t$ , in the reactor are determined by the momentum balance, which is given as follows:

$$m \frac{dv}{dt} = f_a + f_c + g \quad (1)$$

$$I \frac{d\omega}{dt} = T \quad (2)$$

where  $m$  is the mass of the particle,  $v$  and  $\omega$  are the translational and rotational velocities, respectively,  $I$  is the moment of inertia,  $f_a$  is the force acting on a particle exerted by the surrounding fluid,  $f_c$  is the contact force,  $g$  is the gravitational force, and  $T$  is the torque caused by the contact force and the moment of inertia of the particle. Cundall and Strack [17] proposed a sample model to formulate the particle-particle interaction. Based on their research, the contact force between two spherical particles can be modeled by the simple concepts of the spring, the dash-pot, and the friction slider. The contact force  $f_c$  can be divided into a normal contact force  $f_{cn}$  and a tangential contact force  $f_{ct}$ , as follows [18]:

$$f_{cn} = k_n \Delta x_n - \eta_n \frac{dx_n}{dt} \quad (3)$$

$$f_{ct} = k_t \Delta x_t - \eta_t \frac{dx_t}{dt} \quad \text{if } |f_{ct}| \leq \mu_f |f_{cn}| \quad (4)$$

$$f_{ct} = \mu_f |f_{cn}| \frac{x_t}{|x_t|} \quad \text{if } |f_{ct}| > \mu_f |f_{cn}| \quad (5)$$

where  $k_n$  and  $k_t$  are the stiffnesses of the springs in the normal and tangential directions, respectively,  $\eta_n$  and  $\eta_t$  are the coefficients of viscous dissipation in the normal and tangential directions, respectively,  $x_n$  and  $x_t$  are the particle displacements in the normal and tangential directions, respectively, and  $\mu_f$  is the friction coefficient. As shown in the above equations, the stiffness, the coefficient of viscous dissipation, and the friction coefficient, which can be obtained from the physical properties of the particles, must be determined before the calculation of the contact force. In the present study, these parameters were determined by the method proposed in the previous papers [19]. Moreover, the stiffness of the springs in the tangential direction

$k_t$  is assumed to be equal to  $k_n$ , and the coefficient of viscous dissipation in the tangential direction  $\eta_t$  is also assumed to be equal to  $\eta_n$ . Here, the contact force model is also used to simulate the interaction between the particle and the wall.

##### 4.2 Liquid phase

The liquid phase is treated as a continuous phase and is modeled in a manner similar to that used in the conventional two-fluid model. The governing equations are the conservation of mass and conservation of momentum equations in terms of the local mean variables over a computational cell, which is given as follows:

$$\frac{\partial \varepsilon}{\partial t} + \nabla \cdot (\varepsilon \mathbf{u}) = 0 \quad (6)$$

$$\frac{\partial (\rho_g \varepsilon_g \mathbf{u})}{\partial t} + \nabla \cdot (\rho_g \varepsilon_g \mathbf{u} \mathbf{u}) = -\varepsilon_g \nabla p + f_{a,i} + \varepsilon_g (\mu + \mu_e) \nabla^2 \mathbf{u} \quad (7)$$

where  $\varepsilon_g$  is the void fraction,  $\mathbf{u}$  is the velocity vector of the fluid,  $p$  is the pressure of the fluid,  $f_a$  is the fluid drag force exerted on the particle,  $\mu$  is the fluid viscosity,  $\mu_e$  is the eddy viscosity,  $\delta V$  is the volume of the computational cell, and  $n$  is the number of particles inside the cell. Here, the standard  $k$ - $\varepsilon$  model is used as the turbulence model. The turbulent kinetic equation and dissipation rate equation are as follows:

$$\rho_g \left( \frac{\partial k}{\partial t} + (\mathbf{v} \cdot \nabla) k \right) = \nabla \cdot \left( \left( \mu + \frac{\mu_e}{\sigma_k} \right) \nabla k \right) + s - \rho_g \varepsilon \quad (8)$$

$$\rho_g \left( \frac{\partial \varepsilon}{\partial t} + (\mathbf{v} \cdot \nabla) \varepsilon \right) = \nabla \cdot \left( \left( \mu + \frac{\mu_e}{\sigma_\varepsilon} \right) \nabla \varepsilon \right) + c_1 \frac{\varepsilon}{k} s - c_2 \rho_g \frac{\varepsilon^2}{k} \quad (9)$$

where

$$\mu_e = \rho_g C_\mu k^2 / \varepsilon \quad (10)$$

$$s = 2\mu_e \left( \frac{\partial u_i}{\partial x_j} \right)^2 \quad (11)$$

The relative constants in the turbulent model are listed in Table 1. The fluid drag force can be calculated as follows:

$$f_{a,i} = \beta (v_{pi} - u_i) \delta V \quad (12)$$

where  $v_p$  is the particle velocity. The coefficient  $\beta$  can be determined by Ergun's equation ( $\varepsilon \leq 0.8$ ) [12] or Wen and Yu's equation ( $\varepsilon > 0.8$ ) [13]. In the present study,  $\beta$  was deduced based on the equations summarized in previous studies [14].

Table 1 Constants used in the turbulent model

$C_\mu$	$c_1$	$c_2$	$\sigma_k$	$\sigma_\varepsilon$
0.09	1.44	0.92	1.0	1.3

### 4.3 Simulation condition

In the present simulation, the flow of air and particles is assumed to be two-dimensional because the thickness of the bed is equal to the particle diameter, which is much less than the bed width. The simulation model was designed as microchannel. The liquid phase is injected from inlet A and ejected from an outlet. Microparticles can only leave the calculation domain through the outlet. The cell size for the calculation of liquid motion is  $2.5 \mu\text{m} \times 1.5 \mu\text{m}$ .

Table 2 shows the basic simulation parameter condition of the present study. The time step for simulation is calculated by the equation proposed by Tsuji et al. [18]. The time step strongly depends on the stiffness. The actual stiffness will yield a very small time step, which requires a very long computation time. In the present simulation, a smaller stiffness value was assumed in order to reduce the computation time. The time step for the simulation is  $2 \times 10^{-5}$  s when the particle diameter is  $15 \mu\text{m}$  and  $2 \times 10^{-6}$  when the particle diameter is  $3 \mu\text{m}$ . A no-slip condition is used for the air phase at the walls and particles are allowed for frontal collisions with the wall. Air is injected into the container uniformly in order to fluidize the particles. The results presented in the present paper are obtained in such a state.

Table 2 Basic simulation parameters

Liquid phase		Micro particle phase	
Fluid	Deionized water	Particle shape:	spherical
Density ( $\text{kg/m}^3$ )	1,000	Density ( $\text{kg/m}^3$ )	1,000
Velocity (m/s)	1.0	Spring constant (N/m)	4.0
Viscosity (kg/ms)	$2.0 \times 10^{-5}$	Friction coefficient	0.3
		Gravity acceleration ( $\text{m/s}^2$ )	-9.8

## 5. RESULT AND DISCUSSION

Figure 8 shows a micrograph of the tap water plus particle flow in the cross-section C of the microchannel. The black areas are the electrodes 1 and 12. The shaded dots are the particles in the center of the microchannel. Figure 9 shows the capacitance value in x-axis pixel of cross-section. The x-axis pixel number 0 means the center of the cross-section. The higher number and the lower number is near the wall. The capacitance value of center is much higher than the capacitance value of wall in the cross-section. It means the microparticle is distributed in the center side of cross-section. Figure 10 shows the capacitance value of one cross-section. The capacitance value is obtained by each image pixels. The microparticle is distributed in the center side. In the figure, red indicates the high capacitance of the microparticle distribution, and blue indicates the low capacitance of liquid distribution. The yellow and the green part is distributed around the boundary between the microparticle and the liquid which is an inevitable error

generated by the micro process tomography. In the Fig.10, the x-axis shows the z-axis pixels in the cross-section, the y-axis shows the y-axis pixels in the cross-section, the z-axis shows the capacitance value. Figure 11 shows the 3D reconstruction image in the cross-section of microchannel. The y-axis and z-axis of 2D cross-section image is reconstructed to the time. The cross-section images displayed were collected every  $0.001 \text{ml/h}$ . The microparticle distribution of microchannel is easily understand from the 3D reconstruction image.

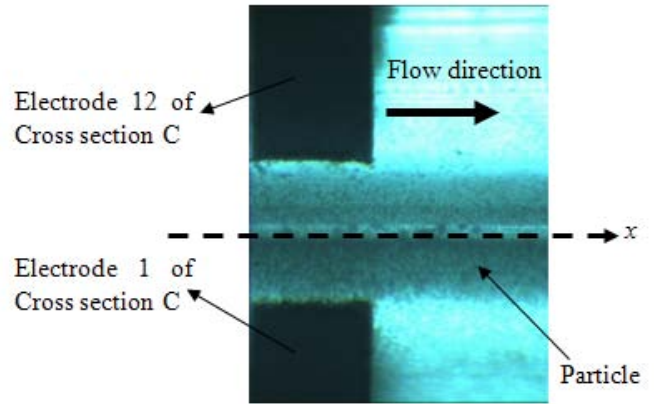


Fig.8 Cross-section image in the microchannel by using ECT

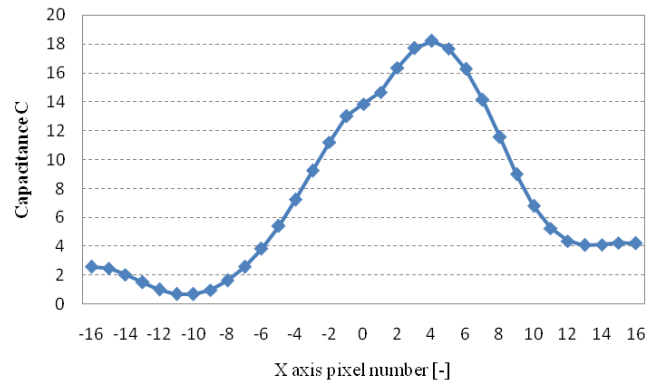


Fig.9 Capacitance value in x-axis pixel in the one cross-section

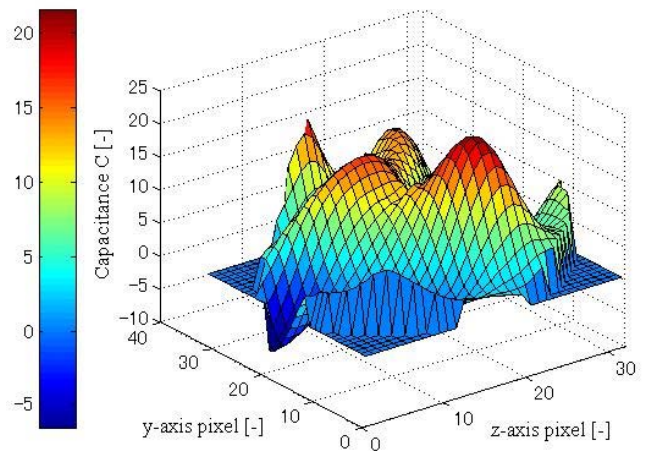


Fig.10 Capacitance value of one cross-section

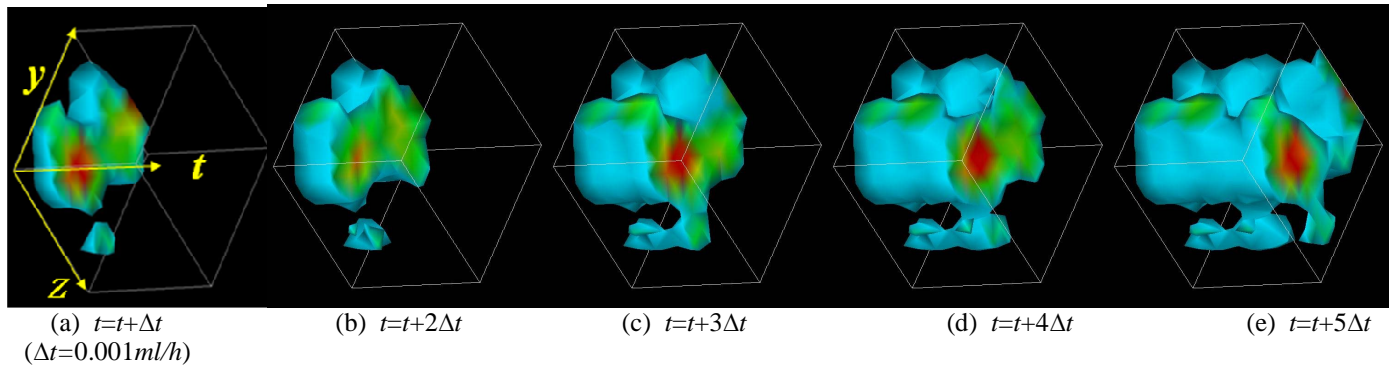
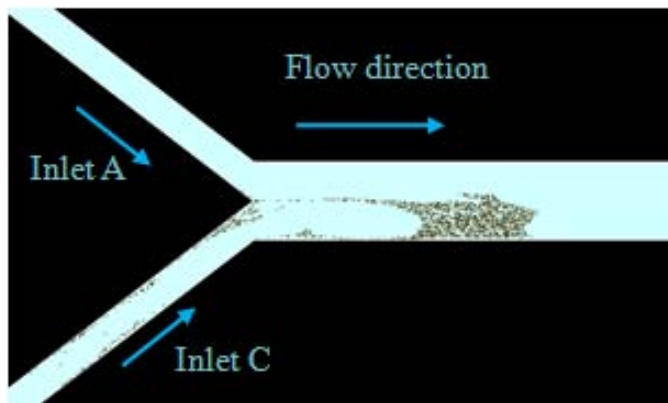
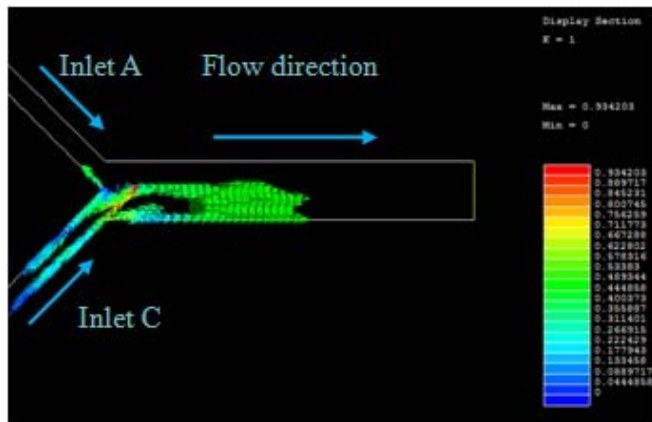


Fig. 11 3D reconstruction image in the cross-section of microchannel

Figure 12 shows the simulation result of microparticle in microchannel. Figure 12(a) shows the microparticle distribution images in the microchannel, whereas the initial microparticle loading condition becomes concentrated and partial. Figure 12(b) shows the microparticle velocity in the microparticle distribution. As the liquid is injected through the inlet A, microparticles start to disperse, and most of the microparticles move toward the outlet area and leave the container through the outlet, although the microparticles concentrate at the center side.



(a) Microparticle distribution



(b) Microparticle velocity

Fig. 12 Simulation result of microparticle in microchannel

## 6. CONCLUSIONS

This paper describes the fabrication of a microchannel with 60 electrodes and the measured impedance of an electrode in the microchannel. The manufacturing process for the microchannel is successfully completed by compressing two quartz glass layers with a platinum electrode. The microparticle distribution was measured in the cross-section of microchannel by using micro process tomography. The microparticle distribution is changed to the time. Usually the microparticle is distributed in the center of cross-section.

A numerical simulation for microparticle distribution was performed by combining the discrete element method and computational fluid dynamics in a two-dimensional domain. Distribution images of the microparticle were obtained by the simulation. The microparticles move toward the outlet area and leave the container through the outlet, although some of the microparticles concentrate at the center side.

## ACKNOWLEDGMENTS

The present study was supported in part by the Academic Frontier Promotion Program of the Japan Ministry of Education, Culture, Sports, Science and Technology and by a Grant-in-Aid for Scientific Research from the Japan Society for the Promotion of Science and the Academic Frontier Promotion Program of MEXT Japan (#21360088).

## REFERENCES

- [1] J. Bastemeijer, W. Lubking, F. Laugere, M. Vellekoop, 2002, Electronic protection methods for conductivity detectors in micro capillary electrophoresis devices, *Sensors and Actuators B*, Vol.83, pp. 98-103
- [2] P. Wang, Z. Chen, H.C. Chang, 2006, A new electro-osmotic pump based on silica monoliths, *Sensors and Actuators B*, Vol.113, pp. 500-509
- [3] J. Bryzek, 1996, Impact of MEMS technology on society, *Sensors and Actuators A*, Vol. 56, pp.1-9
- [4] X. Nie, G. D. Doolen, S. Chen, 2004, Lattice-Boltzmann simulations of fluid flows in MEMS, *Journal of Statistical Physics*, Vol.107, pp.279-289
- [5] M. Ichiyangi, S. Sasaki, Y. Sato, K. Hishida, 2009, Micro-PIV/LIF measurements on electrokinetically-driven flow in surface modified microchannels, *Journal of Micromechanics and Microengineering*, Vol.19, pp.1-9
- [6] D.M. Curtin, D.T. Newport, M.R. Davies, 2006, Utilising  $\mu$ -PIV and pressure measurements to determine the viscosity

- of a DNA solution in a micro channel, *Experimental Thermal and Fluid Science*, Vol.30, pp.843-852
- [7] M. Hoffmann, M. Schluter, N. Rabiger, 2006, Experimental investigation of liquid-liquid mixing in T-shaped micromixers using  $\mu$ -LIF and  $\mu$ -PIV, *Chemical Engineering Science*, Vol.61, pp. 2968-2976
- [8] R.A. Williams, M.S. Beck (Eds.), 1995, Process Tomography, Principles, Techniques and Applications, Butterworth Heinemann, Oxford
- [9] M. Takei, 2006, GVSPM image reconstruction for capacitance CT images of particles in a vertical pipe and comparison with the conventional method, *Measurement Science and Technology*, Vol.17, pp.2104-2112
- [10] Takei M., Ochi M., Saito Y., 2004, "Image Extraction of Particle Concentration at the Plug Front Using 3D Wavelets and comparison with LDV", *Powder Technology*, Vol.142, pp.70-78
- [11] Takei M., Doh D.H., Ochi M., 2008, "Electrical CT image reconstruction technique for power flow in petroleum refinery process", *Experiments in Fluids*, Vol.44, pp.481-490
- [12] T. Dyakowski, 1996, Process tomography applied to multiphase measurement, *Measurement Science and Technology*, Vol.7 pp. 343-353
- [13] H. Griffiths, M.G. Tucker, J. Sage, W.G. Hrennden-Harker, 1996, An electrical impedance tomography microscope, *Physiology Measurement*, Vol.17 pp.15-24
- [14] T.A. York, L. Sun, C. Gregory, J. Hatfield, 2004, Silicon-based miniature sensor for electrical tomography, *Sensors and Actuators A*, Vol.110, pp. 213-218
- [15] T.A. York, T.N. Phua, L. Reichelt, A. Pawlowski, R. Kneer, 2006, A miniature electrical capacitance tomography, *Measurement Science and Technology*, Vol.17, pp. 2119-2129
- [16] P. Yao, G.J. Schneider, D.W. Parther, 2005, Fabrication of microchannel using planar photolithography, *Microfabrication Technologies*, Vol.5718, pp.73-81
- [17] P.A. Cundall and O.D.L. Strack, 1979, A discrete numerical model for granular assemblies, *Geotechnique*, Vol.29, pp. 47-65
- [18] Y. Tsuji, T. Tanaka, T. Ishida, 1992, Lagrangian numerical simulation of plug flow of cohesionless particles in horizontal pipe, *Powder Technology*, Vol.71, pp.239-250
- [19] Y. Tsuji, T. Kawaguchi, T. Tanaka, 1993, Discrete particle simulation of two-dimensional fluidized bed, *Powder Technology*, Vol.77, pp.79-87